Discrete Breather and Soliton-Mode Collective Excitations in Bose-Einstein Condensates in a Deep Optical Lattice with Tunable Three-body Interactions

Galal Ahmed Alakhaly and Bishwajyoti Dey

Department of Physics, University of Pune,

Pune-411007, India.

Abstract: We have studied the dynamic evolution of the collective excitations in Bose-Einstein condensates in a deep optical lattice with tunable three-body interactions. Their dynamics is governed by a high order discrete nonlinear Schrodinger equation (DNLSE). The dynamical phase diagram of the system is obtained using the variational method. The dynamical evolution shows very interesting features. The discrete breather phase totally disappears in the regime where the three-body interaction completely dominates over the two-body interaction. The soliton phase in this particular regime exists only when the soliton line approaches the critical line in the phase diagram. When weak two-body interactions are reintroduced into this regime, the discrete breather solutions reappear, but occupies a very small domain in the phase space. Likewise, in this regime, the soliton as well as the discrete breather phases completely disappear if the signs of the two-and three-body interactions are opposite. We have analysed the causes of this unusual dynamical evolution of the collective excitations of the Bose-Einstein condensate with tunable interactions. We have also performed direct numerical simulations of the governing DNLS equation to show the existence of the discrete soliton solution as predicted by the variational calculations, and also to check the long term stability of the soliton solution.

1. Introduction

The unprecedented control over ultra-cold atoms in optical lattices allows the Bose-Einstein condensates (BECs) formed by such atoms to model various physical phenomena. A few examples are Bloch oscillation, superfluid to Mott-insulator transition, Efimov physics etc. Efimov state were first experimentally observed in BECs [1] 35 years after its prediction by Efimov [2]. In the Efimov state of the condensate, the three-body interaction can completely dominate over the two-body interaction. For a very recent paper on the Efimov effect in BECs see [3]. Effective multi-body interactions has also been

experimentally observed in BECs [4]. It is well known that the Feshbach resonance mechanism allows fine tuning of the two-body interactions in BECs. In a recent paper Safavi-Naini et. al. [5] proposed an interesting mechanism for tuning the onsite three-body interaction using Efimov states [2, 6] and its radio frequency (RF) coupling with the triply occupied state. They found that a strong three-body attraction affects the order of the Mott-insulator-superfluid transition. Such RF coupling of the trimer state has also been experimentally observed in ultra cold Fermi gases [7]. Very recently, Daley and Simon suggested an experimental method to make coherent three-body interactions dominate the physics of ultracold lattice gases [8].

BEC exhibit a range of many-body phenomena, such as collective excitations which are significantly affected by the inter-atomic interactions. Soliton and breather modes are examples of such collective excitations. These nonlinear modes are localised in space, and arises due to the balance between nonlinearity and dispersion in the system [9]. Such localised collective modes has been experimentally observed in BECs [10]. These nonlinear collective modes also occurs in nonlinear lattice systems and are known as discrete breathers and discrete solitons. Nonlinear lattices are used to model energy localisation and transport in physics and biology [11]. Collective excitations modes of a fermionic gas of ^{6}Li atoms in the BEC-BCS crossover regime has also been experimentally observed [12] and it shows a critical transition with variation of the strength of inter-atomic interactions. Analytical studies of the effects of two- and three-body inteactions, and also the anharmonicity of the trap potential on the stability and collective excitations of BECs, are also reported in the literature [13]. However not much is known about the localised collective excitation of BECs loaded in an optical lattice. It is natural to ask how the two- and three-body interactions affects the nonlinear localised collective excitations of BECs in a deep optical lattice.

In this paper, we study how the dynamical evolution of the collective excitations in BEC is affected by the presence of local and tunable three-body interactions. For this we obtain the dynamical phase diagram of the system using the time-dependent variational method. We find that the dynamical evolution of the collective excitations of the condensate in the regime where three-body interaction dominates over the two-body interaction shows very unusual and interesting behaviour. We have also performed direct numerical simulations of the governing equation of the system to show the existence of the discrete soliton solutions as predicted by the variational calculations, and also to check the long term stability of such solutions.

The plan of the paper is as follows: In Section 2, we derive the higher order discrete nonlinear Schrodinger equation (DNLS), which describes the dynamics of the scalar BECs in a deep optical lattice. In Section 3, we describe the variational dynamics to study the phase diagram of the system. In Section 4, we report various phases of the system as obtained from the variational analysis and plot the phase diagrams. In Section 5, we report results of the direct numerical simulations of the higher order DNLS equation. Finally we give a conclusion in Section 6.

2. Model

The dynamics of the BEC with two- and three-body interactions is given by the effective mean-field 1D *quintic* time dependent Gross-Pitaevskii (GP) equation or the nonlinear Schrodinger equation (NLS)

$$i\hbar\frac{\partial\Phi}{\partial t} = -\frac{\hbar^2}{2m}\nabla^2\Phi + [v_{ext} + g_0 \mid \Phi \mid^2 + g_2 \mid \Phi \mid^4]\Phi \tag{1}$$

where g_0 and g_2 are the coupling constants for the two- and three-body interactions which depend on the s-wave scattering length a and the atomic mass. The condensate is trapped in an optical lattice potential given by $v_{ext} = U_l(x,y)\sin^2(2\pi z/\lambda)$ where λ is the wave-length of the laser, $\lambda/2$ is the lattice spacing of the optical lattice and $U_l(x,y)$ is determined by the intensity of the laser beam. Eq. (1) has been derived from various approaches such as renormalisation group approach [14], from many-body Schrodinger equation [15] and also from microscopic theory [16]. For the deep optical lattice (for large enough laser power) one can use the tight-binding approximation, where the strongly localised wave functions (atomic orbitals) at the well of the lattice can be approximated by the Wannier functions. Accordingly, we write the condensate order parameter $\Phi(\mathbf{r},t)$ as a linear combination of the atomic orbitals (LCAO) $\phi(\mathbf{r} - \mathbf{r}_n) = \phi_n(\mathbf{r})$ localised in the trap n as

$$\Phi(\mathbf{r},t) = \sqrt{N_T}\sum_n \psi_n(t)\phi(\mathbf{r} - \mathbf{r}_n) \tag{2}$$

where N_T is the total number of atoms. The orthonormal conditions of the atomic orbitals (Wannier functions) gives

$$\int d\mathbf{r}\phi_n(\mathbf{r})\phi_{n+1}(\mathbf{r}) = 0$$
$$\int d\mathbf{r}\phi_n^2(\mathbf{r}) = 1 \tag{3}$$

3

where $\psi_n(t)$ is the n-th amplitude which can be written in terms of the number of particles N_n and phases θ_n in trap n as

$$\psi_n(t) = \sqrt{\rho_n(t)}e^{i\theta_n(t)} \tag{4}$$

where $\rho_n = N_n/N_T$. For the tight-binding approximation (Eq. (2)) to be valid, the depth of the optical lattice should be much larger than the chemical potential μ and the energy of the system should be confined to the lowest band [17]. Substituting Eq. (2) in equation Eq. (1), the GP equation reduces to the discrete nonlinear Schrodinger equation (DNLSE) with higher order nonlinearity [18, 19, 20]

$$i\frac{\partial \psi_n}{\partial t} = -\frac{1}{2}(\psi_{n-1} + \psi_{n+1}) + (\epsilon_n + \Lambda_0 \mid \psi_n \mid^2 + \Lambda_2 \mid \psi_n \mid^4)\psi_n \tag{5}$$

where

$$\Lambda_0 = \frac{g_0 N_T}{2K} \int d\mathbf{r}[\phi_n^4], \tag{6}$$

$$\Lambda_2 = \frac{g_2 N_T^2}{2K} \int d\mathbf{r}[\phi_n^6] \tag{7}$$

and

$$\epsilon_n = \frac{1}{2K} \int d\mathbf{r}[\frac{\hbar^2}{2m}(\nabla\phi_n)^2 + v_{ext}\phi_n^2]. \tag{8}$$

Here time has been rescaled as $t \to \frac{\hbar}{2K}t$, where

$$K = -\int d\mathbf{r}[\frac{\hbar^2}{2m}\nabla\phi_n \cdot \nabla\phi_{n\pm1} + \phi_n v_{ext}\phi_{n\pm1}], \tag{9}$$

Eq. (5) can be obtained from the Hamiltonian equation of motion

$$\dot{\psi}_n = \frac{\partial H}{\partial(i\psi_n^*)} \tag{10}$$

where the Hamiltonian function is given by

$$H = \sum_n [-\frac{1}{2}(\psi_n\psi_{n+1}^* + \psi_n^*\psi_{n+1}) + \epsilon_n \mid \psi_n \mid^2 + \frac{\Lambda_0}{2} \mid \psi_n \mid^4 + \frac{\Lambda_2}{3} \mid \psi_n \mid^6] \tag{11}$$

with $i\psi_n^*$ and ψ_n as conjugate variables. Both the Hamiltonian and the norm $\sum_n \mid \psi_n \mid^2 = 1$ are conserved.

4

3. Variational Dynamics

We study the dynamics of the BEC using the time-dependent variational method. The basic idea is to take a trial function which depends on a number of time-dependent parameters, and to derive equations of motion for these parameters using the variational principle. The amplitude of the wavefunction determines the density distribution, while its phase determines the velocity field. As mentioned above, the interaction between the particles leads to collective behaviour of the many particle system. It is therefore useful to write the variational wavefunction in terms of variational parameters, such as a center-of-mass coordinate and the width of the condensate, hence describing the collective behaviour of the condensate [21]. For this, we study the dynamical evolution of a Gaussian profile wave packet [18, 22, 23]

$$\psi_V^n(t) = \sqrt{k}.exp\left\{-\frac{(n-\zeta)^2}{\gamma^2} + ip(n-\zeta) + i\frac{\delta}{2}(n-\zeta)^2\right\} \tag{12}$$

where the variational parameters $\zeta(t)$ and $\gamma(t)$ are the center and the width respectively of the density $\rho_n = |\psi_n|^2$, $p(t)$ and $\delta(t)$ are their associated momenta, and k is a normalisation factor. The linear site dependence of the phase term shows that the velocity or the conjugate momentum of the center-of-mass coordinate $\zeta(t)$ is site independent. Similarly the quadratic site dependence of the phase term shows that the velocity or the conjugate momentum of the width $\gamma(t)$ depends linearly on site n [21]. The dynamical evolution of the variational wavepacket can be obtained by a variational on the Lagrangian

$$L = \sum_{n=-\infty}^{n=\infty} i\dot{\psi}_n\psi_n^* - H \tag{13}$$

Using Eqs. (11) and (12), and after rearrangement, L can be written as

$$L = p\dot{\zeta} - \frac{\gamma^2\dot{\delta}}{8} - \left[\frac{\Lambda_0}{2\sqrt{\pi}\gamma}\right] - \left[\frac{2\Lambda_2}{3\sqrt{3}\pi\gamma^2}\right] + \cos pe^{-\eta} - V(\gamma,\zeta) \tag{14}$$

where

$$\eta = \frac{1}{2\gamma^2} + \frac{\gamma^2\delta^2}{8} \tag{15}$$

and

$$V = k\int dn[\epsilon_n e^{-2(n-\zeta)^2/\gamma^2}] \tag{16}$$

5

The equation of motion for the variational parameters q_i, where $q_i = p, \zeta, \gamma$ and δ, can be obtained from the Euler-Lagrange equations

$$\frac{d}{dt}\left(\frac{\partial L}{\partial \dot{q}_i}\right) = \frac{\partial L}{\partial q_i} \tag{17}$$

as

$$\dot{p} = -\frac{\partial V}{\partial \zeta} \tag{18}$$

$$\dot{\zeta} = \sin(p)e^{-\eta} \tag{19}$$

$$\dot{\delta} = (\frac{4}{\gamma^4} - \delta^2)\cos p\, e^{-\eta} + \frac{2\Lambda_0}{\sqrt{\pi}\gamma^3} + \frac{16\Lambda_2}{3\sqrt{3}\pi\gamma^4} - \frac{4}{\gamma}\frac{\partial V}{\partial \gamma} \tag{20}$$

and

$$\dot{\gamma} = \gamma\delta\cos p\, e^{-\eta} \tag{21}$$

The pairs (ζ, p) and $(\frac{\gamma^2}{8}, \delta)$ are canonically conjugate dynamical variables with respect to the effective Hamiltonian

$$H = \frac{\Lambda_0}{2\sqrt{\pi}\gamma} + \frac{2\Lambda_2}{3\sqrt{3}\pi\gamma^2} - \cos p\, e^{-\eta} + V(\gamma, \zeta) \tag{22}$$

The wave packet group velocity is given by

$$v_g \equiv \frac{\partial H}{\partial p} \tag{23}$$

and the inverse effective mass is given by

$$\frac{1}{m^*} = \frac{\partial^2 H}{\partial p^2} = \cos p\, e^{-\eta} \tag{24}$$

The numerical solutions of the above coupled nonlinear ODEs (Eqs. (18-21)) along with the Hamiltonian (Eq. (22)) gives the dynamical regimes or phases of the system (Eq. (5)). Knowing the solutions, various phases can be obtained as follows: as mentioned above, γ and δ are conjugate variables. γ represent the width of the wavepacket and δ denote its conjugate momenta. A plot of $\delta(t)$ versus $\gamma(t)$ gives the corresponding phase space $(\delta - \gamma)$ trajectory. To obtain the soliton phase, we note that the solitons are shape-preserving nonlinear localised solutions. This means that the width of the soliton solution do not change with time. A soliton solution can be obtained

6

by imposing the condition $\dot{\gamma} = \dot{\delta} = 0$. This implies that the soliton mode is be represented by the fixed point of the $\delta - \gamma$ trajectory. The discrete breathers are nonlinear collective excitations which are localised in space and oscillates in time. This implies that for the discrete breather solutions, the width $\gamma(t)$ and its conjugate momenta $\delta(t)$ will oscillate in time and the corresponding $\delta - \gamma$ trajectories will be closed curves. Similarly, for the self-trapped phase the motion of the center of the wave packet stops $(\dot{\zeta} \to 0)$ as the effective mass tends (Eq. (24)) to infinity. On the other hand, for the diffusive phase there is complete spreading of the wave packet and this phase corresponds to $\gamma \to \infty$, $\dot{\zeta} \neq 0$, therefore the effective mass is finite. Various phases as obtained from the solutions of Eqs. (18-21) can be shown in the phase diagram.

4. Phase diagram

For a horizontal optical potential, the onsite energy ϵ_n, as well as $V(\zeta, \alpha)$, are constant [18]. Accordingly from Eq. (18) the momentum $p(t)$ is conserved. This implies $p(t) = p_0$ where p_0 is the initial momentum. From Eq. (22) the conserved initial energy can be written as

$$H_0 = \frac{\Lambda_0}{2\sqrt{\pi\alpha}} + \frac{2\Lambda_2}{3\sqrt{3}\pi\alpha} - \cos p_0 e^{-\frac{1}{2\alpha} - \frac{\alpha\delta^2}{8}} \tag{25}$$

For the sake of convenience we have denoted the width of the wave packet by α instead of γ, where $\alpha = \gamma^2$. Eq. (25) can be rewritten as

$$\delta^2 = -\frac{\left[8\alpha \log\left(\frac{\frac{\Lambda_0}{2\sqrt{\pi\alpha}} + \frac{2\Lambda_2}{3\sqrt{3}\pi\alpha} - H_0}{\cos p_0} \right) + 4 \right]}{\alpha^2} \tag{26}$$

The trajectories in the $(\alpha - \delta)$ plane can be obtained from the above equation along with the solutions of the coupled equations, Eqs. (18-21). In the region $\cos p_0 > 0$, there are two phases. This can be seen as follows: since the argument of the logarithm term in Eq. (26) has to be positive, this implies that for $H_0 > 0$ the width $\alpha(t)$ can attain a maximum value α_{max} for $t \to \infty$. The value of α_{max} can be obtained by equating the argument of the logarithm term to zero. When $\alpha \to \alpha_{max}$, we obtain from Eq. (26) that $\delta \to \infty$. Eq. (15) then implies $\eta \to \infty$ and accordingly we obtain from Eq. (19) that $\dot{\zeta} \to 0$, and from Eq. (24), that $1/m^* \to 0$. This corresponds to the self-trapped phase since the centre of the wave packet

stops as the effective mass goes to infinity. Thus we see that even if the system is fully Hamiltonian (conservative), the apparent damping occurs due to the fast (exponential) growth of the effective mass with time. On the other hand, when $-\cos p_0 < H_0 < 0$, we see from Eq. (26) that in this case $\alpha(t \to \infty) \to \infty$, and accordingly $\delta \to 0$ and from Eq. (15) $\eta \to 0$. But from Eq. (19) $\dot{\zeta} \neq 0$ and from Eqs. (24) and (25) we see that the effective mass is finite as $\frac{1}{m^*} \approx -H_0 > 0$. There is complete spreading of the wave packet, giving rise to the diffusive phase. The critical line which separates the self-trapped and the diffusive phases is obtained from the condition $H_0 = 0$. Substituting $H_0 = 0$ in Eq. (25), we get the critical line (with $\delta_0 = 0$) as

$$\Lambda_{0,c} = 2\sqrt{\pi\alpha_0}\left(\cos p_0 e^{-1/2\alpha_0} - \frac{2\Lambda_2}{3\sqrt{3}\pi\alpha_0}\right) \tag{27}$$

The critical line for $\cos p_0 > 0$ is shown in Fig. 1.

The negative effective mass ($\cos p_0 < 0$) case is more interesting. This is because in this case, beside the self-trapping and the diffusion regimes, we get two new phases. These are the discrete soliton and discrete breather phases. In this case, the conserved initial energy H_0 and the equation for the $(\alpha - \delta)$ trajectory are same as Eq. (25) and Eq. (26) respectively, except that the $\cos p_0$ terms in these two equations should be replaced by $-|\cos p_0|$. Following the same procedure as discussed above, we can see that in this case there are also self-trapping and diffusion regimes, and the critical line separating these two regimes is obtained from the condition $H_0 = |\cos p_0|$. Replacing H_0 by $|\cos p_0|$ in the expression of the conserved Hamiltonian, we obtain the critical line which separates the two regimes as

$$\Lambda_{0,c} = 2\sqrt{\pi\alpha_0}\left(|\cos p_0|(1 - e^{-1/2\alpha_0}) - \frac{2\Lambda_2}{3\sqrt{3}\pi\alpha_0}\right) \tag{28}$$

As mentioned above, the soliton mode is represented by the fixed point of the $\alpha - \delta$ trajectory ($\dot{\alpha} = 0$ and $\dot{\delta} = 0$). Eqs. (20) and (21) then have stationary solution $\alpha(t) = \alpha_0$ and $\delta(t) = 0$ ($\alpha(t) = \gamma^2(t)$). From Eqs. (15) and (19), we obtain that $\dot{\zeta} = \sin(p_0)e^{-\frac{1}{2\alpha_0}} = \text{constant}$. This implies that for soliton solutions, the center of mass moves with constant velocity, and the width (shape) of the soliton do not change with time. From Eq. (20) we then obtain

$$\Lambda_{0,\text{soliton}} = 2\sqrt{\frac{\pi}{\alpha_0}}\left(|\cos p_0|e^{-1/2\alpha_0} - \frac{4\Lambda_2}{3\sqrt{3}\pi}\right) \tag{29}$$
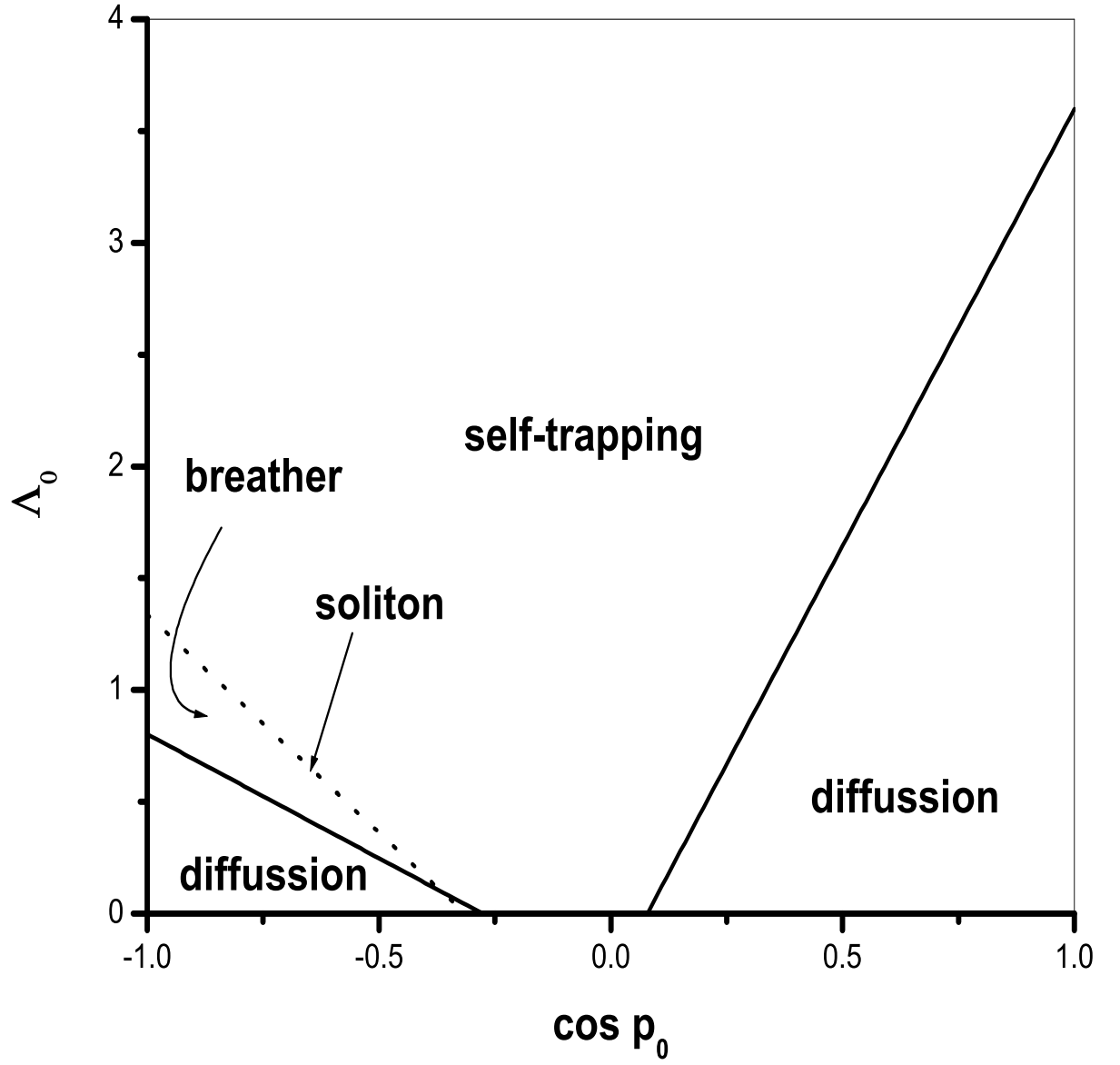
Figure 1: Dynamical phase diagram with two- and three-body interactions $(\Lambda_2 = 1)$ with $\alpha_0 = 2$, $\delta_0 = 0$ and $\zeta_0 = 0$.

This gives the soliton line in the phase diagram. The soliton line gives the value of the two-body interaction parameter Λ_0 for which the soliton solutions are allowed. It may be noted that the soliton line corresponds to the maximum of the energy (Eq. (22)). This is because Eq. (29) can also be obtained from the condition $\left(\frac{\partial H}{\partial \alpha}\right)_{\delta=0,\alpha_0} = 0$ and for which $\left(\frac{\partial^2 H}{\partial \alpha^2}\right)_{\delta=0,\alpha_0} < 0$. The soliton line is shown by the dotted line in Fig. 1. Yet another interesting phase which appears in the case of the negative effective mass is the discrete breather. Discrete breathers are nonlinear collective modes which are localised in space and periodic in time. For discrete breather solution $\alpha(t)$, $\delta(t)$ and m^* oscillates with time. The center of mass travels with nearly constant velocity and with an oscillating width. Discrete breather solution appears when the nonlinearity parameter $\Lambda_{0,c} < \Lambda_0 < \Lambda_{0,\text{soliton}}$. The trajectories in the $\alpha - \delta$ plane are closed and α oscillates between the initial values α_0 and the maximum value $\alpha_{osc}^{max} > \alpha_0$. The complete phase diagram for the case when the two-body interactions dominates over the three-body interactions is shown in Fig. 1.

We can now obtain the phase diagrams for the case when the three-body interaction dominates over the two-body interaction ($\Lambda_2 >> \Lambda_0$). For this, we first consider the case when the three-body interactions completely dominate over the two-body interactions, and accordingly we set the two-body nonlinear interaction parameter $\Lambda_0 = 0$. By substituting $\Lambda_{0,c} = 0$ in Eq. (28), we get the critical line $\Lambda_{2,c}$ which separates the self-trapped and the diffusion regimes as,

$$\Lambda_{2,c} = \frac{3\sqrt{3}\pi\alpha_0}{2} \left|\cos p_0\right| \left(1 - e^{-1/2\alpha_0}\right) \tag{30}$$

Similarly, by substituting $\Lambda_{0,\text{soliton}} = 0$ in Eq. (29) we get the soliton line as

$$\Lambda_{2,\text{soliton}} = \frac{3\sqrt{3}\pi}{4} \left|\cos p_0\right| e^{-1/2\alpha_0} \tag{31}$$

The soliton solutions are expected when the three-body interaction parameter Λ_2 values are on the soliton line, i.e. $\Lambda_2 = \Lambda_{2,\text{soliton}}$. From the above equation we can see that this can be satisfied for arbitrary value of α_0 (initial width of the condensate density). We checked this prediction of the variational calculations by direct numerical simulations of the governing equation of the system, the DNLS equation (Eq. (5)). However, from the direct numerical
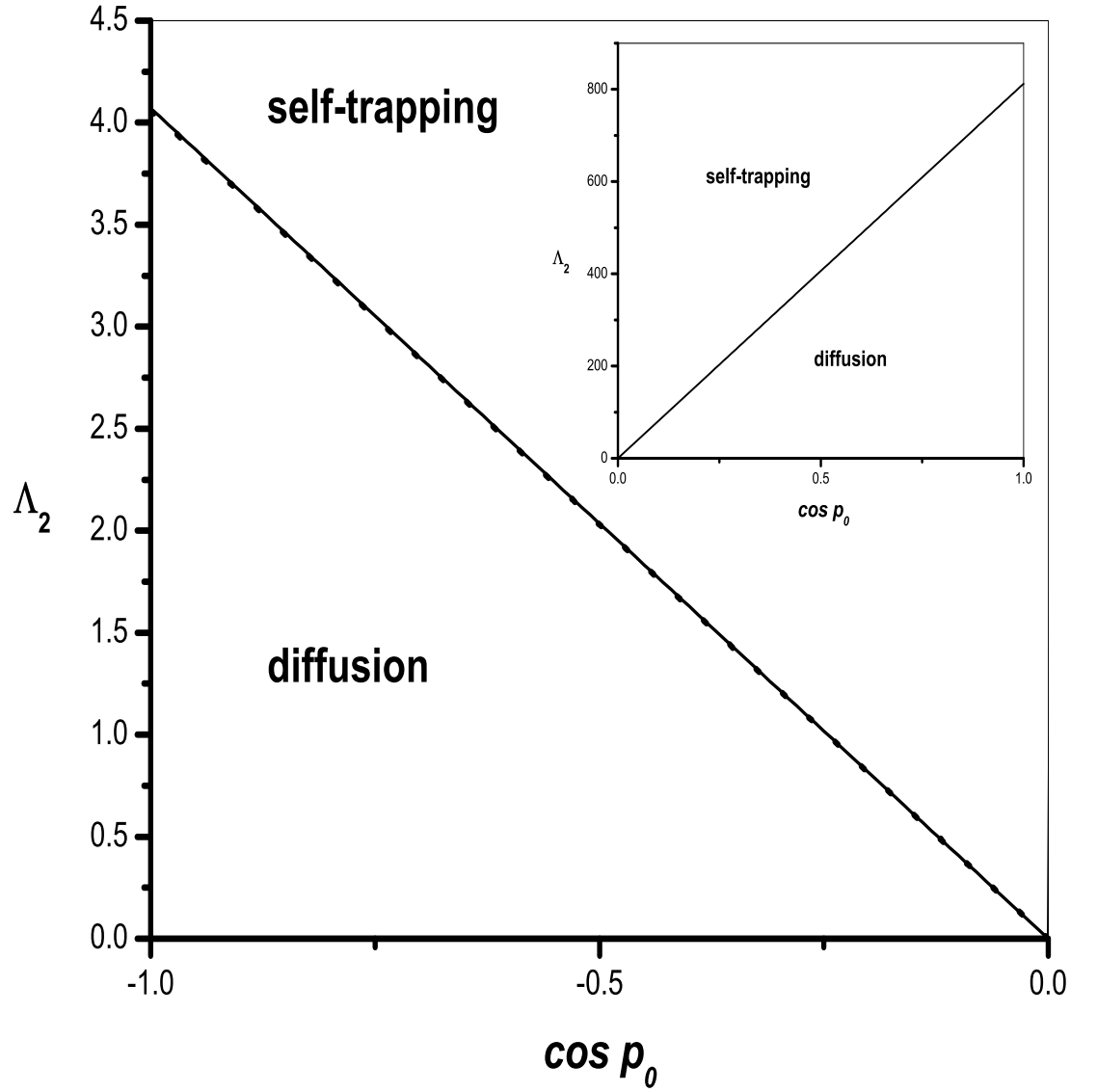
Figure 2: Dynamical phase diagram of the BEC with only three-body interaction ($\Lambda_2 > 0$ and $\Lambda_0 = 0$) with $\alpha_0 = 100$, $\delta_0 = 0$ and $\zeta_0 = 0$. The solid line represent the critical line ($\Lambda_{0,\mathrm{c}}$) and the overlapping dotted line represent the soliton line ($\Lambda_{0,\mathrm{soliton}}$). The inset show the phase diagram for $\cos p_0 > 0$.
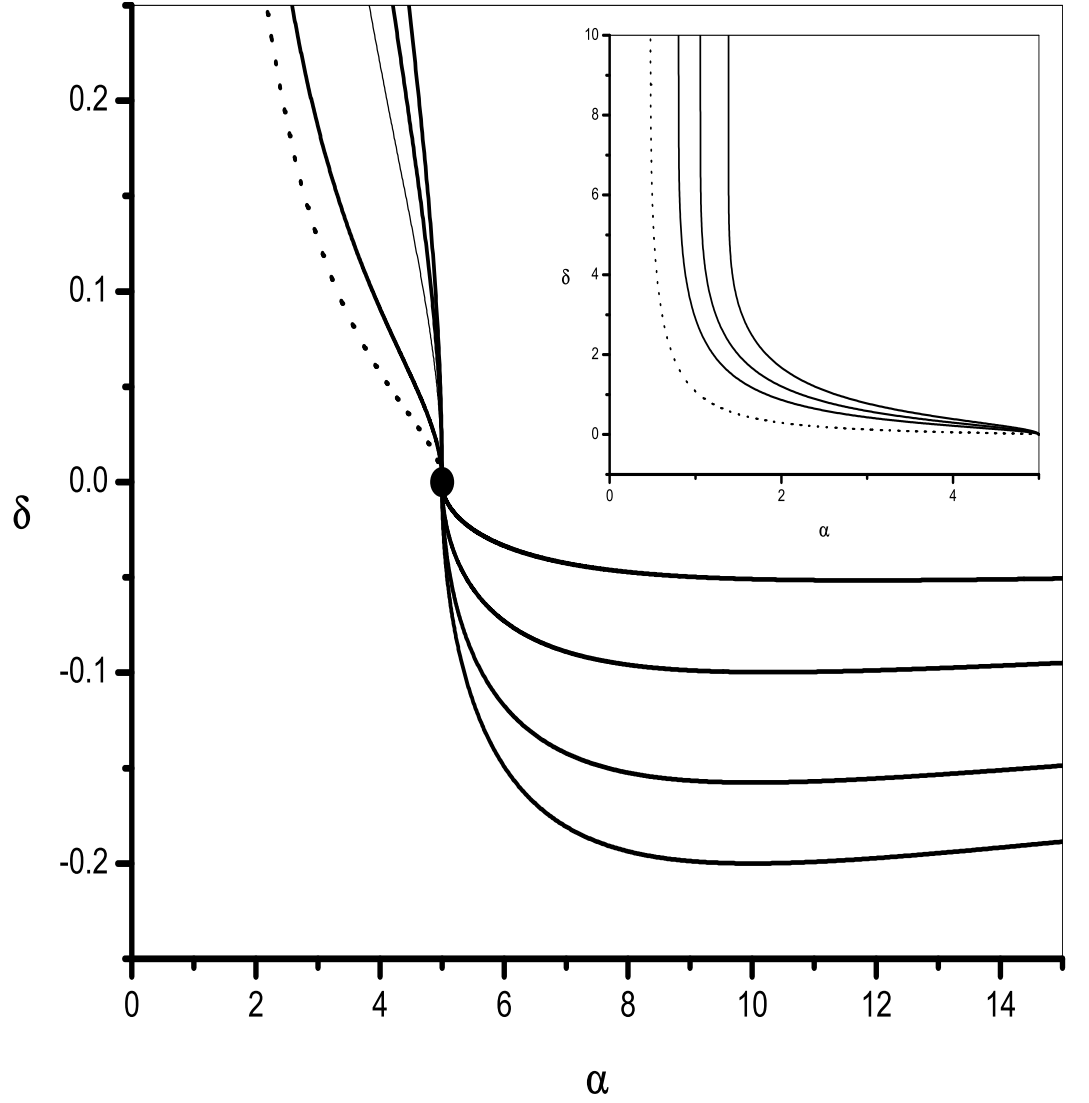
Figure 3: $\alpha - \delta$ trajectories in the state with only three-body interaction ($\Lambda_2 > 0$ and $\Lambda_0 = 0$). the figures are plotted for different values of $\Lambda_2 > 0$ and $\cos p_0 < 0$ with $\alpha_0 = 5$, $p_0 = 3\pi/4$. The critical values of the three-body interaction parameter for different transitions are $\Lambda_{2,c} = 2.7462$ and $\Lambda_{2,\text{soliton}} = 2.61112$. Inset shows the $\alpha - \delta$ trajectories for Λ_2 very close to $\Lambda_{2,\text{soliton}}$.

integration (Section 5) of Eq. (5) we obtain an unusual result that the discrete soliton mode collective excitations exist only for the large value of α_0. From Eqs. (30) and (31) we see that for large value of α_0, $\Lambda_{2,\text{soliton}} \to \Lambda_{2,\text{c}}$, i.e. the soliton solutions exist only when the soliton line approaches the critical line in the phase diagram. Fig. 2 shows the phase diagram for large value of $\alpha_0 = 100$ and we can see that in this case the soliton line (dotted line) approaches the critical line (solid line). From the direct numerical solution of the DNLS equation we find that indeed, there is a stable soliton solution for $\alpha_0 = 100$. Details are given in Section 5. Yet another unusual result for the BEC with only three-body interactions is that it does not allow discrete breather collective mode excitations. The absence of the discrete breather modes in this regime can be seen from the following: discrete breather collective modes occur when the three-body interaction parameter Λ_2 satisfies the relation $\Lambda_{2,\text{c}} < \Lambda_2 < \Lambda_{2,\text{soliton}}$. As mentioned above, the trajectories in the $\alpha - \delta$ plane are closed, and $\alpha(t)$ oscillates between the initial value α_0 and the maximum value $\alpha_{\text{osc}}^{\max} > \alpha_0$. The breather region extends until the value of parameter Λ_2 approaches $\Lambda_{2,\text{breather}}$. For $\Lambda_{2,\text{soliton}} < \Lambda_2 < \Lambda_{2,\text{breather}}$, α_0 oscillates between α_0 and the minimum value $\alpha_{\text{osc}}^{\min} < \alpha_0$. Both the values $\alpha_{\text{osc}}^{\max}$ and $\alpha_{\text{osc}}^{\min}$ are roots (together with α_0) of Eq. (26) for $\Lambda_0 = 0$ and $\cos p_0 < 0$. The condition for which this equation does not have another root $\alpha_{osc}^{min} < \alpha_0$ gives $\Lambda_{0,\text{breather}}$ [18]. After rearrangement, one can show that $\Lambda_{2,\text{breather}}$ is given by the maximum value of the r.h.s of the expression

$$\frac{\Lambda_2}{\Lambda_{2,\text{soliton}}} = \frac{2\alpha_0 x}{(1-x)} \left[1 - e^{(x-1)/2\alpha_0 x} \right] \tag{32}$$

Here $\alpha_{\text{osc}}^{\min} = x\alpha_0$ and $x < 1$. From the maximum value of the r.h.s, we find that $\Lambda_{2,\text{breather}} \to \Lambda_{2,\text{soliton}}$. When $\Lambda_{2,\text{breather}} \to \Lambda_{2,\text{soliton}}$, the area enclosed within the $\alpha - \delta$ trajectories shrinks to zero (to the soliton fixed point) implying nonexistence of the discrete breather modes. Also, for the three-body interaction parameter in the range $\Lambda_{2,\text{c}} < \Lambda_2 < \Lambda_{2,\text{soliton}}$ there are no closed trajectories in the $\alpha - \delta$ plane and this implies that there are no discrete breather solutions. This is shown in Fig. 3, where we can see that there are no closed trajectories around the soliton fixed point. The inset of this figure shows no closed trajectories very close to $\Lambda_{2,\text{soliton}}$. However, if we now add a weak two-body interaction ($\Lambda_0 < \Lambda_2$), and if both the parameters Λ_0 and Λ_2 are positive, then the discrete breather solution is allowed. In this case, after rearrangement, we obtain
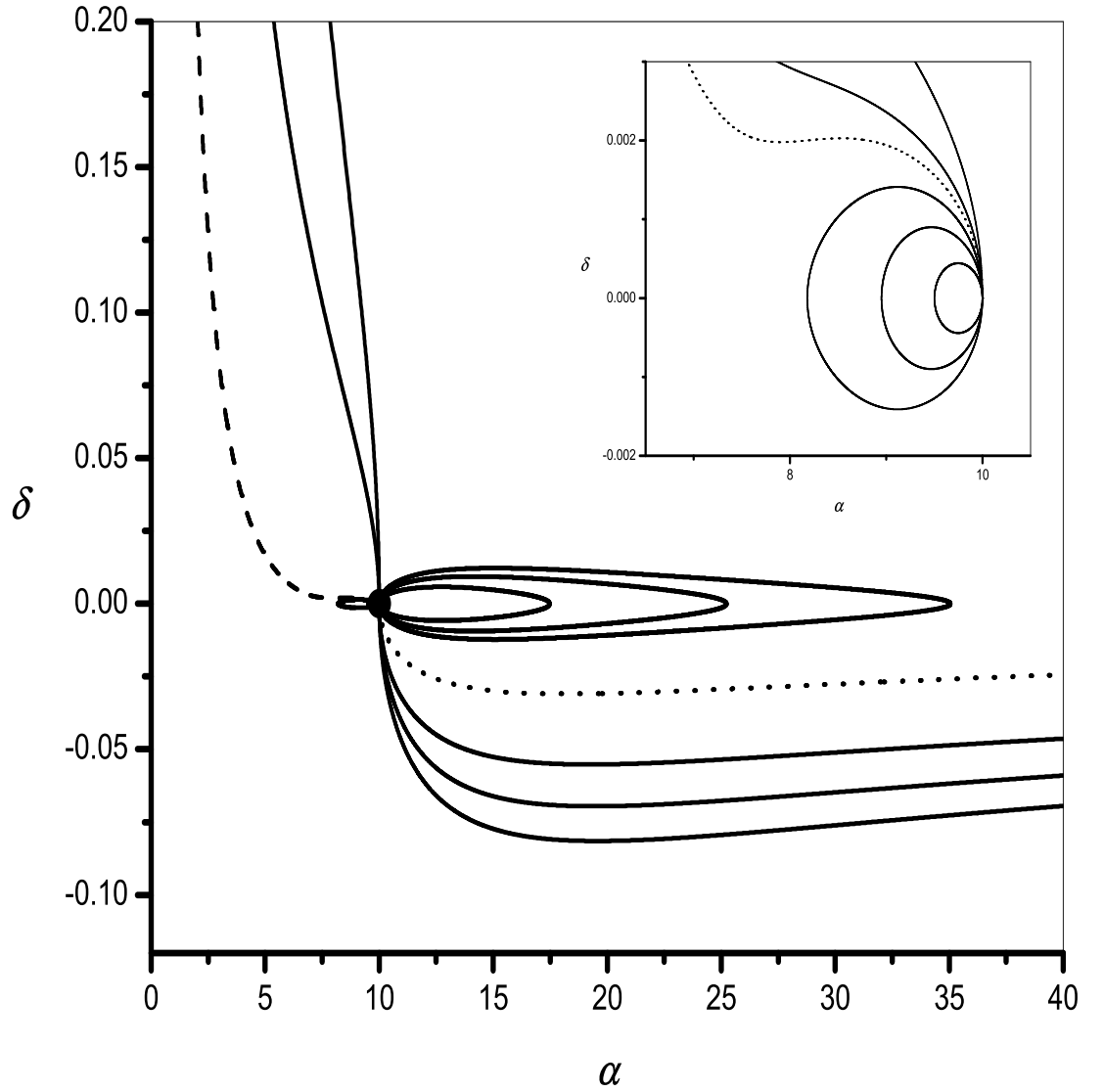
Figure 4: $\alpha - \delta$ trajectories in the state with weak two-body interaction ($\Lambda_2 > \Lambda_0$) for different values of $\Lambda_2 > 0$ (beginning from the bottom $\Lambda_2 = 0.5, 1, 1.5, \Lambda_{2,c}, 2.32, 2.34, 2.36, \Lambda_{2,\text{soliton}}, 2.382, 2.384, \Lambda_{2,\text{breather}}, 4, 10$) for the case $\cos p_0 < 0$ with $\alpha_0 = 5$, $p_0 = 3\pi/4, \Lambda_0 = 0.1$. Inset shows the $\alpha - \delta$ trajectories close to $\Lambda_{2,\text{breather}}$ (from the top $\Lambda_{2,c} = 2.39, 2.386, \Lambda_{2,\text{breather}}, 2.384, 2.383, 2.382$).

$$\frac{\Lambda_2}{\Lambda_{2soliton}} = \frac{\frac{2\alpha_0 x}{(1-x)}\left[1 - e^{(x-1)/2\alpha_0 x}\right] + \frac{\sqrt{\alpha_0}\sqrt{x}\left(1-\sqrt{x}\right)}{\sqrt{\pi}(1-x)\cos p_0 e^{-1/2\alpha_0}}\Lambda_0}{1 + \frac{\sqrt{\alpha_0}}{2\sqrt{\pi}\cos p_0 e^{-1/2\alpha_0}}\Lambda_0} \qquad (33)$$

Again, from the maximum value of the r.h.s of Eq. (33) we find that $\Lambda_{2,\text{breather}} > \Lambda_{2,\text{soliton}}$, thus satisfying the condition for the appearance of the discrete breather solutions. This is shown in Fig. 4, where we can see that there are closed trajectories (on the right of the soliton fixed point) representing the discrete breather solutions. For $\Lambda_2 > \Lambda_{2,\text{soliton}}$, but very close to $\Lambda_{2,\text{soliton}}$, the area of the trajectories near the fixed point is very small but nonzero (shown in the inset of Fig. 4), thus allowing the discrete breather solutions to exist. Fig. 5 shows the complete phase diagram.

When Λ_0 have an opposite sign to that of Λ_2, then both the solutions, soliton as well as the discrete breather, are not allowed. The absence of the soliton and breather modes in this case is due to the fact that $\Lambda_{2,\text{soliton}}$ is much smaller than that of $\Lambda_{2,c}$ and accordingly the $\Lambda_{2,\text{soliton}}$ (soliton line) lies deep inside the diffusion region. Due to the exponential dependence of $\Lambda_{2,\text{soliton}}$ on α_0 (Eq. (31)), it is not possible to increase α_0 till the $\Lambda_{2,\text{soliton}}$ line cross the $\Lambda_{2,c}$ critical line for the soliton solution to reappear. Similarly, the discrete breather solutions are also not allowed in this case since $\Lambda_{2,\text{breather}}$ (breather line) also lies well below the $\Lambda_{2,c}$ critical line.

5. Numerical solutions of the higher order discrete nonlinear Schrodinger equation

We have also solved the higher order DNLS equation (Eq. (5)) directly using numerical procedures. This verifies the existence of the discrete soliton solutions in presence of only three-body interactions, as predicted by the variational analysis. We have also checked the stability of the soliton solutions over a long time scale. We write $\psi_n(t) = \sqrt{\rho_n(t)}e^{i\theta_n(t)}$ in terms of its two components, as $\psi_n = (x_n, y_n)$ and $\dot{\psi}_n = (\dot{x}_n, \dot{y}_n)$. Here x_n and y_n denote the real and imaginary parts respectively of ψ_n. In terms of these variables, the DNLS (Eq. (5)) can be written as the coupled equations

$$\dot{x}_n = -\frac{1}{2}(y_{n-1} + y_{n+1}) + \epsilon_n y_n + \Lambda_0(x_n^2 + y_n^2)y_n + \Lambda_2(x_n^2 + y_n^2)^2 y_n \qquad (34)$$

and

$$\dot{y}_n = \frac{1}{2}(x_{n-1} + x_{n+1}) - \epsilon_n x_n - \Lambda_0(x_n^2 + y_n^2)x_n - \Lambda_2(x_n^2 + y_n^2)^2 x_n \qquad (35)$$
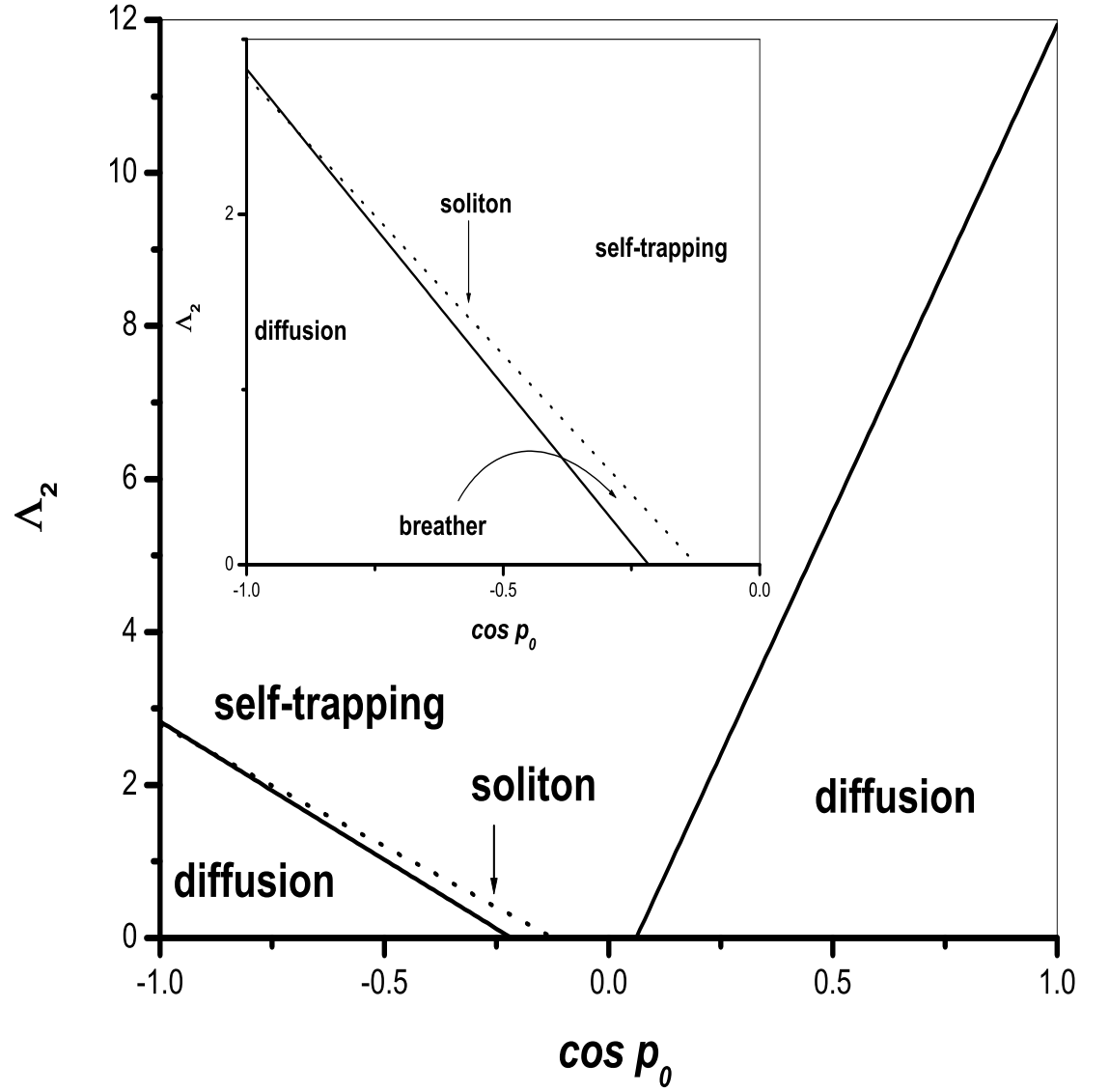
15

Figure 5: Dynamical phase diagram in the state for positive two- and three-body interactions with $\alpha_0 = 2, \delta_0 = 0, \zeta_0 = 0$ and weak two-body interaction parameter $\Lambda_0 = 0.24$. Inset shows the small discrete breather region.

Since we want to compare the numerical results with the variational results, we take the initial condition as the variational wavefunction (Eq. (12)) and accordingly write the initial values of (x_n, y_n) as

$$x_n = \sqrt{k} e^{-\frac{(n-\zeta)^2}{\alpha}} \cos\left[p(n-\zeta) + \frac{\delta}{2}(n-\zeta)^2\right] \qquad (36)$$

and

$$y_n = \sqrt{k} e^{-\frac{(n-\zeta)^2}{\alpha}} \sin\left[p(n-\zeta) + \frac{\delta}{2}(n-\zeta)^2\right] \qquad (37)$$

where $\alpha = \gamma^2$. We solve the coupled nonlinear equations (Eqs.(34, 35)) using the Runge-Kutta method, with the initial conditions given by Eqs.(36, 37). The constants of motion, the Hamiltonian (Eq. (11)) and the norm were checked at every time step of the numerical integration to verify that these remained constant over time. To connect the numerical results with that of the variational results, we calculate relevant parameters which shows the existence of the soliton solutions. Thus we calculate the numerical average position which is defined as

$$<n> = \sum_n n |\psi_n|^2 \qquad (38)$$

It is easy to show that $<n> = \zeta(t)$. As mentioned above (Eq. (12)), $\zeta(t)$ is the variational parameter which denote the average position or the center of the density $\rho_n = |\psi_n|^2$. We also calculate the numerical width of the wave packet $2\sqrt{<n^2>}$ which is defined as

$$<n^2> = \sum_n n^2 |\psi_n|^2 - <n>^2 \qquad (39)$$

Again, it can be shown that $<n^2> = \gamma^2(t)/4 = \alpha(t)/4$. As mentioned above, $\alpha(t)$ is variational parameter which denote the width of the wave packet (Eq. (12)). For the soliton solution to exist, the width $<n^2>$ should not change with time. Fig. 6 shows a stable soliton mode collective excitation as obtained from the direct numerical integration of the DNLS equation (Eq. (5)) for $\alpha_0 = 100$. From the figure we can see that the shape of the soliton solution do not change with time. The inset shows the average position and the width over a long interval of time. This confirms the long term stability of the discrete soliton solution.
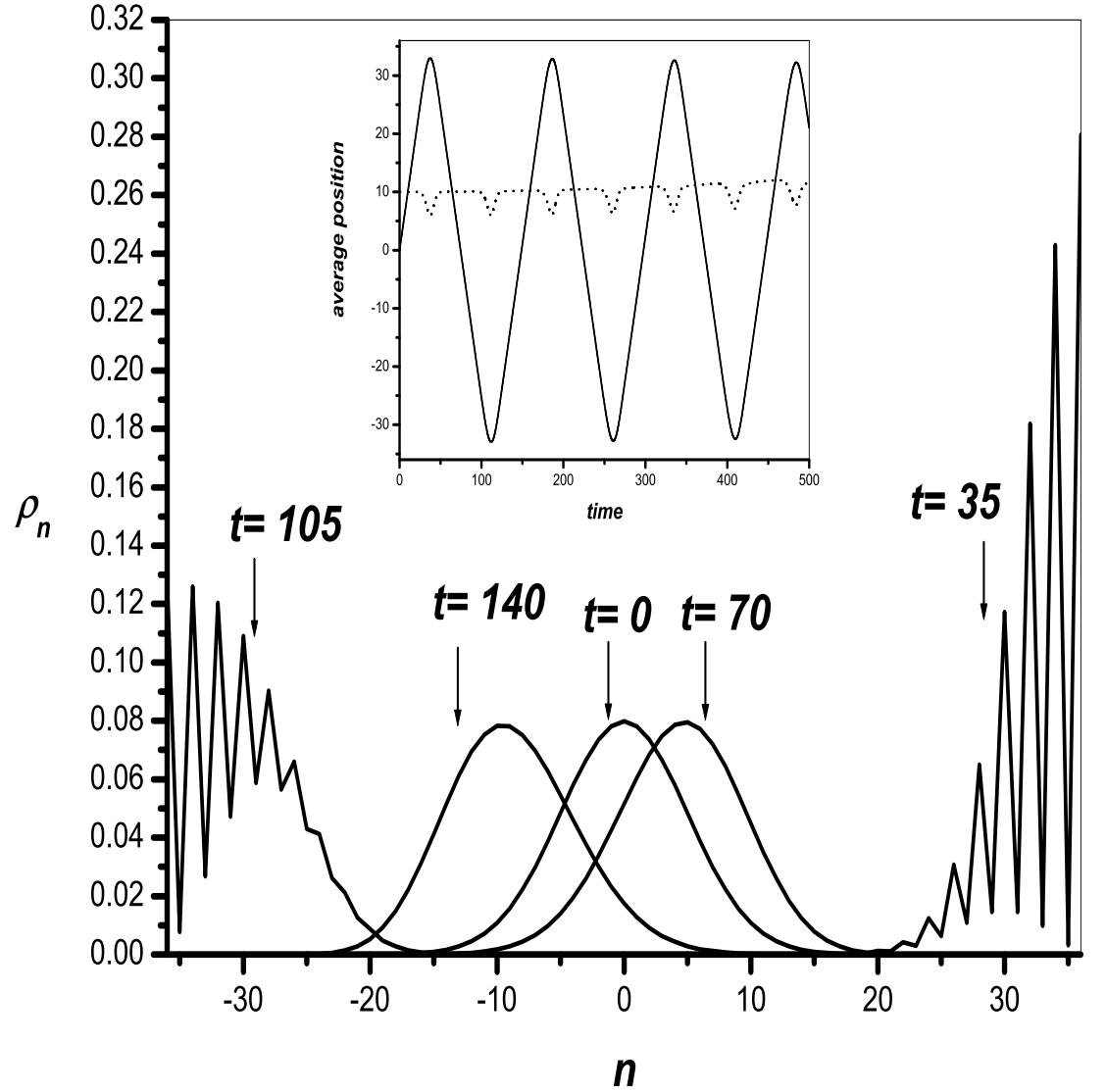
17

Figure 6: Density profile of the soliton solution in the state with only three-body interaction ($\Lambda_2 > 0$ and $\Lambda_0 = 0$) obtained numerically at different time intervals $t = 0, 35, 70, 105$ and 140 for $\alpha_0 = 100$, $p_0 = 1.6$ in finite array of 73 sites. Inset shows the width (dotted line) and average position (solid line) for a much longer time interval.

6. Conclusion

In conclusion, we have studied BECs in a deep optical lattice with a tunable three-body interaction. We have obtained the dynamical phase diagram of the system analytically, using the time-dependent variational method. The phase diagrams shows interesting dynamical evolution of the collective excitations with variation of the strength as well as the sign (attractive or repulsive nature) of the two- and three-body interactions. We have explained the causes of the appearance of the phase diagrams of the system. We have also solved the dynamical equation of the system, the higher order discrete nonlinear Schrodinger equation (DNLSE), numerically, to check the existence of the soliton solution in the presence of only three-body interactions, as predicted by the variational analysis. As mentioned above, BECs where the three-body interactions dominate over the two-body interactions have been prepared experimentally. It should therefore be possible experimentally to look for the dynamical evolution of the collective modes of BECs as discussed above.

References

[1] T. Kraemer *et al*, Nature **440**, 315 (2006).

[2] V. Efimov, Phys. Lett. **33B**, 563 (1970).

[3] B. Huang *et al*, Phys. Rev. Lett. **112**, 190401 (2014).

[4] S. Will *et al*, Nature **465**, 09036 (2010).

[5] A. Safavi-Naini *et al*, Phys. Rev. Lett. **109**, 135302 (2012).

[6] F. Ferlaino and R. Grimm, Physics **3**, 9 (2010).

[7] T. Lompe *et al*, Science **330**, 940 (2010).

[8] A.J. Daley and J. Simon, Phys. Rev. A **89**, 053619 (2014).

[9] L. Pitaevskii and S. Stringari *Bose-Einstein Condensation* , Oxford University Press, Oxford (2003).

[10] B. Eiermann *et al*, Phys. Rev. Lett. **92**, 230401 (2004).

[11] R. Sarkar and B. Dey, Phys. Rev. E **76**, 016605 (2007) and references therein.

[12] M. Bartenstein *et al*, Phys. Rev. Lett. **92**, 203201 (2004).

[13] Y. Wen-Mei *et al*, Commun. Theor. Phys. **51**, 433 (2009); L. Guan-Qiang *et al*, Phys. Rev. A **74**, 055601 (2006); L. Guan-Qiang *et al*, Commun. Theor. Phys. **50**, 1129 (2008); H. Ji-Xuan, Phys. Lett. A **368**, 366 (2007); L. Hao-Cai *et al*, Chin. Phys. Lett **27**, 030304 (2010); P. Ping and L. Guan-Qiang, Chin. Phys. B **18**, 3221 (2009).

[14] E.B. Kolomeisky, T.J. Newman, J.P. Straley and X. Qi, Phys. Rev. Lett. **85**, 1146 (2000).

[15] E.H. Lieb, R. Seiringer and J. Yngvason, Phys. Rev. Lett. **91**, 150401 (2003).

[16] T. Kohler, Phys. Rev. Lett. **89**, 210404 (2002).

[17] C. Kittel, *Introduction to Solid State Physics*, Seventh Edition, John Wiley and Sons (ASIA) Pte Ltd., Singapore (1996).

[18] A. Trombettoni and A. Smerzi, Phys. Rev. Lett. **86**, 2353 (2001); A. Trombettoni and A. Smerzi, J.Phys. B: At. Mol. Opt. Phys. **34**, 4711 (2001).

[19] F.Kh. Abdullaev *et al*, Phys. Rev. A **64**, 043606 (2001).

[20] G.L. Alfimov *et al*, Phys. Rev. E **66**, 046608 (2002).

[21] C.J. Pethick and H. Smith, *Bose-Einstein Condensation in Dilute Gases*, Cambridge University Press, Cambridge (2002). Chapter 7.

[22] J.J.G. Ripoli and V.M. Perez-Garcia, Phys. Rev. A **59**, 2220 (1999).

[23] V.M. Perez-Garcia *et al*, Phys. Rev. A **56**, 1424 (1997).